



Hardwood spent mushroom substrate–based activated biochar as a sustainable bioresource for removal of emerging pollutants from wastewater

Alejandro Grimm¹ · Glaydson Simões dos Reis¹ · Van Minh Dinh² · Sylvia H. Larsson¹ · Jyri-Pekka Mikkola^{2,3} · Eder Claudio Lima⁴ · Shaojun Xiong¹

Received: 24 November 2021 / Revised: 14 March 2022 / Accepted: 21 March 2022 / Published online: 2 April 2022
© The Author(s) 2022

Abstract

Hardwood spent mushroom substrate was employed as a carbon precursor to prepare activated biochars using phosphoric acid (H_3PO_4) as chemical activator. The activation process was carried out using an impregnation ratio of 1 precursor:2 H_3PO_4 ; pyrolysis temperatures of 700, 800, and 900 °C; heating rate of 10 °C min^{-1} ; and treatment time of 1 h. The specific surface area (SSA) of the biochars reached 975, 1031, and 1215 $\text{m}^2 \text{g}^{-1}$ for the samples pyrolyzed at 700, 800, and 900 °C, respectively. The percentage of mesopores in their structures was 75.4%, 78.5%, and 82.3% for the samples pyrolyzed at 700, 800, and 900 °C, respectively. Chemical characterization of the biochars indicated disordered carbon structures with the presence of oxygen and phosphorous functional groups on their surfaces. The biochars were successfully tested to adsorb acetaminophen and treat two simulated pharmaceutical effluents composed of organic and inorganic compounds. The kinetic data from adsorption of acetaminophen were fitted to the Avrami fractional-order model, and the equilibrium data was well represented by the Liu isotherm model, attaining a maximum adsorption capacity of 236.8 mg g^{-1} for the biochar produced at 900 °C. The adsorption process suggests that the pore-filling mechanism mainly dominates the acetaminophen removal, although van der Waals forces are also involved. The biochar produced at 900 °C removed up to 84.7% of the contaminants in the simulated effluents. Regeneration tests using 0.1 M NaOH + 20% EtOH as eluent showed that the biochars could be reused; however, the adsorption capacity was reduced by approximately 50% after three adsorption–desorption cycles.

Keywords Hardwood spent mushroom substrate · Phosphoric acid activation · Biochars · Acetaminophen adsorption · Pore-filling mechanism · Pharmaceutical effluents

1 Introduction

Pharmaceuticals are a large and diverse group of human and veterinary medicinal compounds used in large quantities worldwide [1]. These types of chemicals are classified as emerging pollutants, i.e., synthetic or natural substances generated by human activities that may cause ecological impacts but are not included in routine monitoring programs. However, depending on their (eco)toxicity, potential health effects, and occurrence, these compounds may be candidates for future regulation [2, 3]. Pharmaceuticals are chemicals designed to alter the body's metabolic processes, functions, and structures for the patient's benefit. The drugs are metabolized mainly through the liver and digestive system; however, this process does not occur in 100%. This means that metabolized and free forms of the drugs are excreted and end up in wastewater that in urban areas is commonly

✉ Alejandro Grimm
alejandro.grimm@slu.se

✉ Glaydson Simões dos Reis
glaydson.simo.es.dos.reis@slu.se;
glaydsonambiental@gmail.com

¹ Department of Forest Biomaterials and Technology, Swedish University of Agricultural Sciences, 90183 Umeå, Sweden

² Technical Chemistry, Department of Chemistry, Chemical-Biological Center, Umeå University, 90187 Umeå, SE, Sweden

³ Industrial Chemistry and Reaction Engineering, Johan Gadolin Process Chemistry Centre, Åbo Akademi University, 20500 Åbo-Turku, FI, Finland

⁴ Institute of Chemistry, Federal University of Rio Grande Do Sul (UFRGS), Av. Bento Gonçalves 9500, Porto Alegre 91501-970, Brazil

transported to sewage treatment plants. Apart from this, solid waste treatment plants equipped with suitable technology for recycling or destruction of harmful chemicals are uncommon in most countries, and pharmaceuticals that are past the expiration date are often disposed of together with household garbage or flushed in toilets, which leads to increased pressure on the environment. Pharmaceutical compounds, such as cancer and psychiatric drugs, antibiotics, analgesics, and anti-inflammatories, among others, have been found in rivers [4], surface waters [5], and groundwater [6]. Leachates from municipal solid waste landfill sites have also been described as the cause of surface and groundwater contamination [7, 8]. Research studies have found that the continuous presence of pharmaceuticals in surface water, even in concentrations of $\mu\text{g L}^{-1}$ or ng L^{-1} , has the potential to over time interact with organisms and cause a wide range of ecological and human health problems [9, 10].

Conventional urban sewage water treatment, based on biological processing and activated sludge, is usually unable to remove residual concentrations of all kinds of pharmaceuticals [11], meaning that some drugs always make it into the fresh waters of rivers, lakes, and seas. Advanced treatments to reduce the concentration of emerging pollutants in water include the following: ozonation, which is usually incapable of removing common persistent micropollutants such as X-ray contrast media [12]. Membrane technologies are available in a wide span of options adapted for different applications, but the running costs of using this technology depend on water-quality issues [13]. The solar photo-Fenton method, by itself, is used to degrade organic contaminants, but it needs to be combined with other methods based on adsorption to obtain water free of degradation products [14, 15]. Photo-Fenton electrochemical degradation is quite an unexplored and complex technology that involves the use of chemicals and expensive equipment [16]. Photolysis, photocatalysis, and photodegradation lead to degradation products and require expensive equipment [17–19]. Electrochemical oxidation also requires the use of chemicals and expensive equipment [20]. Different treatments based on biosorption using algae and fungi are not very efficient, and the possibility of regenerating the biosorbent is minimal [21]. Adsorption using different materials based on clay minerals is an efficient option for the removal of contaminants from water, but the adsorbent production methods and raw materials are usually expensive [22–24]. Therefore, most of these technologies represent an unrealistic solution in underdeveloped and developing countries.

Research has shown that filters based on activated carbon made of precursors such as different types of biomasses are a good option for the removal of emerging pollutants from water [25–28]. This type of technology has several advantages, such as initial low implementation and operation costs, and the removal effectiveness can reach 100%. This

urges the development of water cleaning methods based on inexpensive and widely available biomass residues.

White-rot fungi such as *Pleurotus* spp. and *Lentinula edodes*, among others, are commonly cultivated on substrates made of hardwood sawdust and have the ability to use cellulose, hemicellulose, and lignin as carbon sources. The edible mushroom industry represents a multimillion-dollar industry. China is one of the largest producers and exporters of edible mushrooms with approximately 80% of the products in the global market, followed by the EU and the USA that stand for approximately 10%. The total global production of edible mushrooms is approximately 34 Mt with a 30-fold increase since 1978, which corresponds to a value of around 34 billion USD [29]. After cultivation, approximately 70 wt% dry mass of the initial substrate usually remains as a waste known as spent mushroom substrate (SMS) [30, 31]. The latter has no commercial value and cannot always be reused within the mushroom production processes and, therefore, represents a problematic waste that needs to be disposed of without generating environmental issues. This type of waste is mainly composed of partially degraded cellulose, hemicellulose, and lignin and could be used as a precursor to produce carbon-based materials to remove emerging contaminants from water.

This paper shows how birch wood-based SMS can be utilized as a precursor for producing high surface area meso/microporous biochars using the chemical activation method with phosphoric acid at different process temperatures. The carbons were characterized for their textural properties by N_2 adsorption–desorption isotherms, and surface functionalities were identified using Raman, Fourier transformed infrared (FT-IR), and X-ray photoelectron spectroscopy (XPS). The surface morphology of the biochars was studied using scanning electron microscopy (SEM). The efficiency of the produced biochars to remove micropollutants from water was examined in batch assays using acetaminophen and synthetic effluents composed of organic and inorganic compounds. The adsorption capacity, kinetics, and adsorption mechanisms were discussed.

2 Materials and methods

2.1 Precursor

Spent mushroom substrate (SMS) was obtained from a previous work where *Pleurotus ostreatus* mushroom was cultivated on different substrates [32]. The SMS used in this work was composed of birch (*Betula* spp.) sawdust and a minor amount of wheat bran. The raw SMS was milled and screen-sieved to obtain a material with homogeneous particle size. Particles with a diameter between 1 and 2 mm were used as carbon precursor to prepare the activated biochars.

2.2 Impregnation and activation process

The precursor used for each experiment (100 g) was mixed with phosphoric acid (50 wt%) using a weight ratio of 1 precursor:2 acid, kneaded to obtain a homogeneous blend and left overnight at room temperature in a sealed container. The activation process was carried out in one step by pyrolysis in an inert atmosphere using a tubular stainless steel reactor (diameter of 100 mm and length of 200 mm) equipped with a thermocouple to measure the temperature of the sample. The reactor was heated externally by an electric muffle furnace. The impregnated precursor was placed in the reactor and heated from room temperature to a final temperature of 700, 800, and 900 °C under N₂ gas flow (500 mL min⁻¹, 99.99%) at a heating rate of 10 °C min⁻¹. The final temperature was kept for 1 h, and after that, the sample was allowed to cool down to a temperature below 150 °C under a N₂ gas flow of 250 mL min⁻¹. Next, the N₂ gas was closed, and the sample was allowed to cool down to room temperature overnight. To remove by-products from the carbonaceous matrix, the produced biochars were washed several times successively with hot water until a neutral pH was attained. The samples were finally dried overnight in an oven at 105 °C to obtain the final product.

2.3 Characterization of the biochars

The textural characterization of the biochars was performed by N₂ adsorption–desorption analysis using Tristar 3000 apparatus, Micrometrics Instrument Corp., Norcross, GA, USA. The samples were first degassed at 110 °C for 3 h under N₂ flow and then measured at liquid N₂ temperature (–196 °C). The specific surface area (SSA) of the samples was calculated by multipoint N₂ sorptiometry using the Brunauer–Emmett–Teller (BET) principle. In addition, pore-volume, average-pore size, and pore size distribution were obtained from sorption isotherms using the Barrett–Joyner–Halenda (BJH) model.

Representative samples of the biochars were analyzed using Raman, Fourier transformed infrared (FT-IR), and X-ray photoelectron spectroscopy (XPS) to identify surface functionalities. The morphology of each biochar was analyzed using scanning electron microscopy (SEM). Raman spectra were collected using a Bruker Bravo handheld spectrometer (Bruker, Ettlingen, Germany) attached to a docking measuring station. The biochar samples were manually ground using an agate mortar and pestle, placed in 5-mL glass vials, and scanned in the 300–3200-cm⁻¹ spectral range at 4 cm⁻¹ resolution for 256 scans. Min–max normalization over the 1000–2000-cm⁻¹ region and smoothing (9 points) was done using the built-in functions of the OPUS software (version 7, Bruker Optik GmbH, Ettlingen, Germany); baseline correction was not needed. FT-IR spectra

were collected with a Bruker IFS 66v/S instrument (Bruker Optics, Germany) in the 4000–400 cm⁻¹ spectral range at 4 cm⁻¹ resolution for 256 scans. Approximately 5 mg of sample was mixed with 400 mg of spectroscopy-grade potassium bromide (KBr) (Uvasol, Merck KGaA, Germany) and manually finely ground using an agate mortar and pestle. Background spectra were collected using pure ground KBr. FT-IR spectra were treated using a 64-point rubber band baseline correction and vector normalization over the 3700–500-cm⁻¹ region using the Opus software. XPS spectra were collected using a Kratos Axis Ultra DLD electron spectrometer using a monochromated Al K_α source operated at 150 W. Analyzer pass energy of 160 eV for acquiring survey spectra and a pass energy of 20 eV for individual photoelectron lines were used. The samples were gently hand-pressed using a clean Ni spatula into a special powder sample holder. Because activated carbon samples are conductive, no charge neutralization system was used. Binding energy (BE) scale was calibrated following the ASTM E2108 and ISO 15472 standards. Processing of the spectra was accomplished with the Kratos software. SEM imaging was carried out using a field-emission scanning electron microscope (FESEM; Zeiss Merlin) with an in-lens secondary electron detector. The instrument was operated at an accelerating voltage of 5 kV and probe current of 100 pA. Samples were attached to carbon tape mounted on aluminum stubs and coated with 2 nm of platinum using a Quorum Technologies Q150T ES device.

2.4 Batch adsorption and regeneration tests

The acetaminophen initial solution concentrations used for the adsorption tests varied from 10 to 1000 mg L⁻¹ at different pH (3.0 to 9.0). Then, aliquots of 20.00 mL of acetaminophen were added to 50.0 mL Falcon flat tubes containing different biochar masses (from 20 to 80 mg). All the adsorption tests were performed at a fixed temperature of 22 °C. First, the Falcon tubes containing acetaminophen and biochars were agitated in a KS250 shaker (IKA Labortechnik) for 1 to 360 min. Afterwards, to separate the biochars from the solutions, the tubes were kept vertical, and a few seconds later, the biochar particles settled down, and with a pipette, the solution was withdrawn; no centrifugation was needed. Next, the residual acetaminophen solutions were measured using a UV–Visible spectrophotometer (Shimadzu 1800) at a maximum wavelength of 243 nm. The adsorption capacity (Eq. 1) and the percentage of acetaminophen removed (Eq. 2) are given below:

$$q = \frac{(C_0 - C_f)}{m} \cdot V \quad (1)$$

$$\% \text{Removal} = 100 \cdot \frac{(C_0 - C_f)}{C_0} \quad (2)$$

where q denotes the removal capacity of acetaminophen adsorbed by the biochars (mg g^{-1}); C_0 the initial acetaminophen concentration in contact with the biochars (mg L^{-1}); C_f the final acetaminophen concentration after adsorption (mg L^{-1}); m the mass of biochars (g); and V the aliquot of the acetaminophen solution (L) introduced in the tube.

The influence of the mass of the biochars on acetaminophen removal was performed using an initial concentration of 200 mg L^{-1} , a contact time of 6 h, natural pH of 6.0, and biochar mass varying from 20 to 80 mg in 20 mL of acetaminophen solution.

To study of the influence of the initial pH, adsorption tests using acetaminophen solutions with an initial concentration of 200 mg L^{-1} and pH ranging from 3.0 to 9.0 were carried out using an adsorbent dosage of 2.0 g L^{-1} and a contact time of 6 h. These experiments were carried out in triplicate. Average values with standard deviation are reported.

For regeneration tests, acetaminophen-laden biochars were washed with water to remove any unadsorbed drug and dried overnight in an oven at 50°C . The dried-laden biochars were contacted with two eluents, i.e., $0.1 \text{ M NaOH} + 20\% \text{ EtOH}$ and $0.25 \text{ M NaOH} + 20\% \text{ EtOH}$ and agitated for 6 h [27]. The desorbed pharmaceutical was then separated from the biochar. The latter was washed with water to remove the eluent and dried overnight in an oven at 50°C . The adsorption capacity of the recycled adsorbent was measured again. A total of four consecutive adsorption–desorption cycles were carried out. This was done in triplicate; average values with standard deviation are reported.

2.5 Models of kinetics and isotherms of adsorption

Pseudo-first-order, pseudo-second-order, and Avrami fractional-order models were used to fit the kinetic data [33–36]. The mathematical equations of these respective models are shown in Eqs. 3, 4, and 5.

$$q_t = q_e \cdot [1 - \exp(-k_1 \cdot t)] \quad (3)$$

$$q_t = \frac{k_2 \cdot q_e^2 \cdot t}{1 + q_e \cdot k_2 \cdot t} \quad (4)$$

$$q_t = q_e \cdot [1 - \exp(-k_{AV} \cdot t)^{n_{AV}}] \quad (5)$$

where t denotes the contact time (min); q_t and q_e are the amount of adsorbate adsorbed at time t and the equilibrium, respectively (mg g^{-1}); k_1 is the pseudo-first-order rate constant (min^{-1}); k_2 the pseudo-second-order rate constant ($\text{g mg}^{-1} \text{ min}^{-1}$); k_{AV} the Avrami fractional-order constant rate (min^{-1}); and n_{AV} the dimensionless Avrami exponent.

Langmuir, Freundlich, and Liu's models were employed for the analysis of equilibrium data; Eqs. 6, 7, and 8 show the corresponding models [33–36].

$$q_e = \frac{Q_{\max} \cdot K_L \cdot C_e}{1 + K_L \cdot C_e} \quad (6)$$

$$q_e = K_F \cdot C_e^{1/n_F} \quad (7)$$

$$q_e = \frac{Q_{\max} \cdot (K_g \cdot C_e)^{n_L}}{1 + (K_g \cdot C_e)^{n_L}} \quad (8)$$

where q_e denotes the adsorbate amount adsorbed at equilibrium (mg g^{-1}); C_e denotes the adsorbate concentration at equilibrium (mg L^{-1}); Q_{\max} denotes the maximum adsorption capacity of the adsorbent (mg g^{-1}); K_L denotes the Langmuir equilibrium constant (L mg^{-1}); K_F denotes the Freundlich equilibrium constant [$\text{mg g}^{-1} (\text{mg L}^{-1})^{-1/n_F}$]; K_g denotes the Liu equilibrium constant (L mg^{-1}); and n_F and n_L are the dimensionless exponents of Freundlich and Liu models, respectively.

The fitting of the kinetic and equilibrium data was evaluated using nonlinear methods, which were evaluated using the Simplex method and the Levenberg–Marquardt algorithm using the fitting facilities of the Microcal Origin 2020 software. The suitability of the kinetic and equilibrium models were evaluated using the determination coefficient (R^2), the adjusted determination coefficient (R^2_{adj}), and the standard deviation of residues (SD) [25, 27, 33, 34] showed in the Eqs. 9, 10, 11 below.

$$R^2 = \left(\frac{\sum_i^n (q_{i,\text{exp}} - \bar{q}_{i,\text{exp}})^2 - \sum_i^n (q_{i,\text{exp}} - q_{i,\text{model}})^2}{\sum_i^n (q_{i,\text{exp}} - \bar{q}_{i,\text{exp}})^2} \right) \quad (9)$$

$$R^2_{\text{adj}} = 1 - (1 - R^2) \cdot \left(\frac{n - 1}{n - p - 1} \right) \quad (10)$$

$$SD = \sqrt{\left(\frac{1}{n - p} \right) \cdot \sum_i^n (q_{i,\text{exp}} - q_{i,\text{model}})^2} \quad (11)$$

In the above equations, $q_{i,\text{model}}$ is the individual theoretical q value predicted by the model; $q_{i,\text{exp}}$ is the individual experimental q value; $\bar{q}_{i,\text{exp}}$ is the average of all experimental q values measured; n is the number of experiments; and p is the number of parameters in the fitting model.

The R^2_{adj} and SD values were used to compare different models of kinetics and equilibrium presented in this work.

The best-fitted model would present the highest R^2_{adj} and lowest SD values [25, 27, 33, 34].

2.6 Simulated pharmaceutical effluents

Two synthetic aqueous effluents made of different pharmaceuticals, as well as other organic and inorganic compounds (Table 1), were used to test the ability of the biochars for treating real effluents. The relative effectiveness of each biochar to remove contaminants from each effluent was calculated based on the area under the UV–Vis spectra before and after the adsorption treatment under the band of absorption from 190 to 800 nm. As was found in other studies [27], this is a quick and simple method that provides an idea of the behavior of the adsorbent during treatment of mixtures of different chemicals even if the λ_{max} of some of the components is outside the measured spectral range.

Table 1 Composition of the two synthetic effluents

Effluent composition	Concentration (mg L ⁻¹)	
	Effluent A	Effluent B
Drugs		
Acetylsalicylic acid	10	20
Propranolol	10	20
Amoxicillin	10	20
Captopril	10	20
Nimesulide	10	20
Diclofenac	10	20
Acetaminophen	20	40
Sugars		
Saccharose	30	50
Glucose	30	50
Other organic components		
Urea	10	20
Citric acid	10	20
Humic acid	10	20
Sodium dodecyl sulfate	5	10
Inorganic components		
Ammonium phosphate	20	30
Ammonium chloride	20	30
Sodium sulfate	10	20
Sodium chloride	50	70
Sodium carbonate	10	20
Calcium nitrate	10	20
Magnesium chloride	10	20
Potassium nitrate	10	20
pH	6	6

3 Results and discussion

3.1 Biochar characterization

3.1.1 Textural properties and morphology

All three biochars displayed the same trend of the N₂ isotherm curve of adsorption/desorption (Fig. 1 a, b, and c), which is closed to the so-called type IV isotherm, according to IUPAC [37]. A type IV isotherm shows hysteresis, which belongs to the mesoporous materials. However, the curves also indicate the presence of some microporosity due to the high N₂ adsorption volume at low pressure. The pyrolysis temperature seemed to have influenced only the total N₂ amount adsorbed.

Although the temperature did not influence the type of the N₂ isotherm, it influenced to a good extent the porosity of the biochar-700, biochar-800, and biochar-900. Table 2 shows that the SSA values increased as the temperature increased. The biochar-900 exhibited the highest SSA equal to 1215 m² g⁻¹.

All three biochars presented a high presence of mesopores on their structures: 75.4%, 78.5%, and 82.3% for biochar-700, biochar-800, and biochar-900, respectively. In addition, the pyrolysis temperature also influenced the total pore volume with values of 0.7086, 0.7163, and 0.8357 cm³ g⁻¹ for biochar-700, biochar-800, and biochar-900, respectively. Thus, most of the total pore volume is composed of the mesopore contribution (see values in Table 2).

The presence of both mesopores and micropores is significant for their use as adsorbents for micropollutant adsorption applications because they have significant and different roles concerning the efficient pollutant diffusion in the pore networks of the adsorbent materials [25, 38, 39].

BJH measurements show the pore size distribution for the three biochars (Fig. 1 d, e, and f). Although the pyrolysis temperature shows no effect on the biochars' pore structure, the samples show similar curves with the prominent peak in the same region at around 3.7 nm; virtually, no pores larger than 30 nm are present in the samples. In addition, the curves show that from 20 nm smaller sizes, the volume adsorption starts to rise to highlight the presence of a large number of large micropores or mesopores from bigger than 2 and smaller than 20 nm.

To examine the influence of the pyrolysis conditions and H₃PO₄ activation on the surface morphology of the biochars, they were subjected to SEM analysis. Figure 2 shows the surface morphology of the three biochars. The SEM images display that all samples present intact structures with roughness and irregular structure with big

Fig. 1 N₂ isotherms (a, b, and c) and pore size distribution (d, e, and f) for the biochars

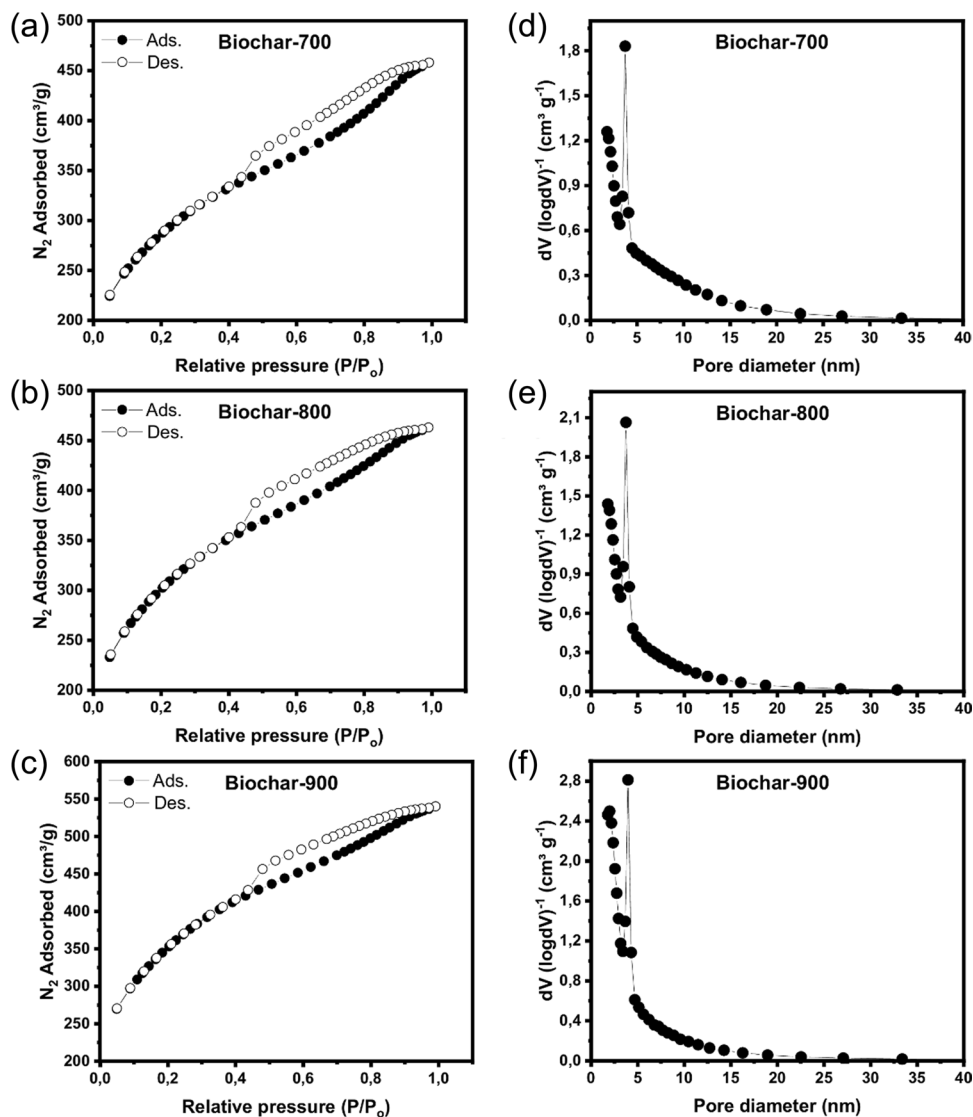


Table 2 Textural properties of the biochars

Parameters	700 °C	800 °C	900 °C
SSA (m ² g ⁻¹)	975	1031	1215
Mesopore surface area (m ² g ⁻¹)	735	809	1000
Mesopore area (%)	75.38	78.47	82.30
Micropore area (m ² g ⁻¹)	240	223	215
Micropore area (%)	24.62	21.63	17.70
Total pore volume (cm ³ g ⁻¹)	0.7086	0.7163	0.8357
Micropore volume (cm ³ g ⁻¹)	0.1199	0.1104	0.1048
Micropore volume (%)	16.92	15.41	12.54
Mesopore volume (cm ³ g ⁻¹)	0.5887	0.6059	0.7309
Mesopore volume (%)	83.08	84.59	87.46
Average pore size (nm)	2.906	2.777	2.751

amounts of holes and cavities that seem to be in a bigger extent for the biochar-800 and biochar-900, which is in accordance with the SSA and pore structure results. By the SEM analysis, it is possible to infer that the pyrolysis temperature (under H₃PO₄ activation) influenced the surface characteristics of the biochars. In addition, the images also show large presence of macropores and ultramacropores; this is very important because if the biochars are used as adsorbent to remove pollutants from waters, they serve as vectors of passage of solution through macropores until it attains smaller pores (in the interior of the biochars).

3.1.2 FTIR, Raman, and XPS analyses

FTIR analysis was carried out to observe how the pyrolysis temperature influenced the presence of chemical functional groups on the biochars' surfaces; it provides valuable information about the chemical surface activity of the biochars.

Fig. 2 SEM images of biochars: **a** biochar-700 at 500× of magnification, **b** biochar-700 at 2 KX of magnification; **c** biochar-800 at 500× of magnification, **d** biochar-800 at 2 KX of magnification; **e** biochar-900 at 500× of magnification, **f** biochar-900 at 2 KX of magnification

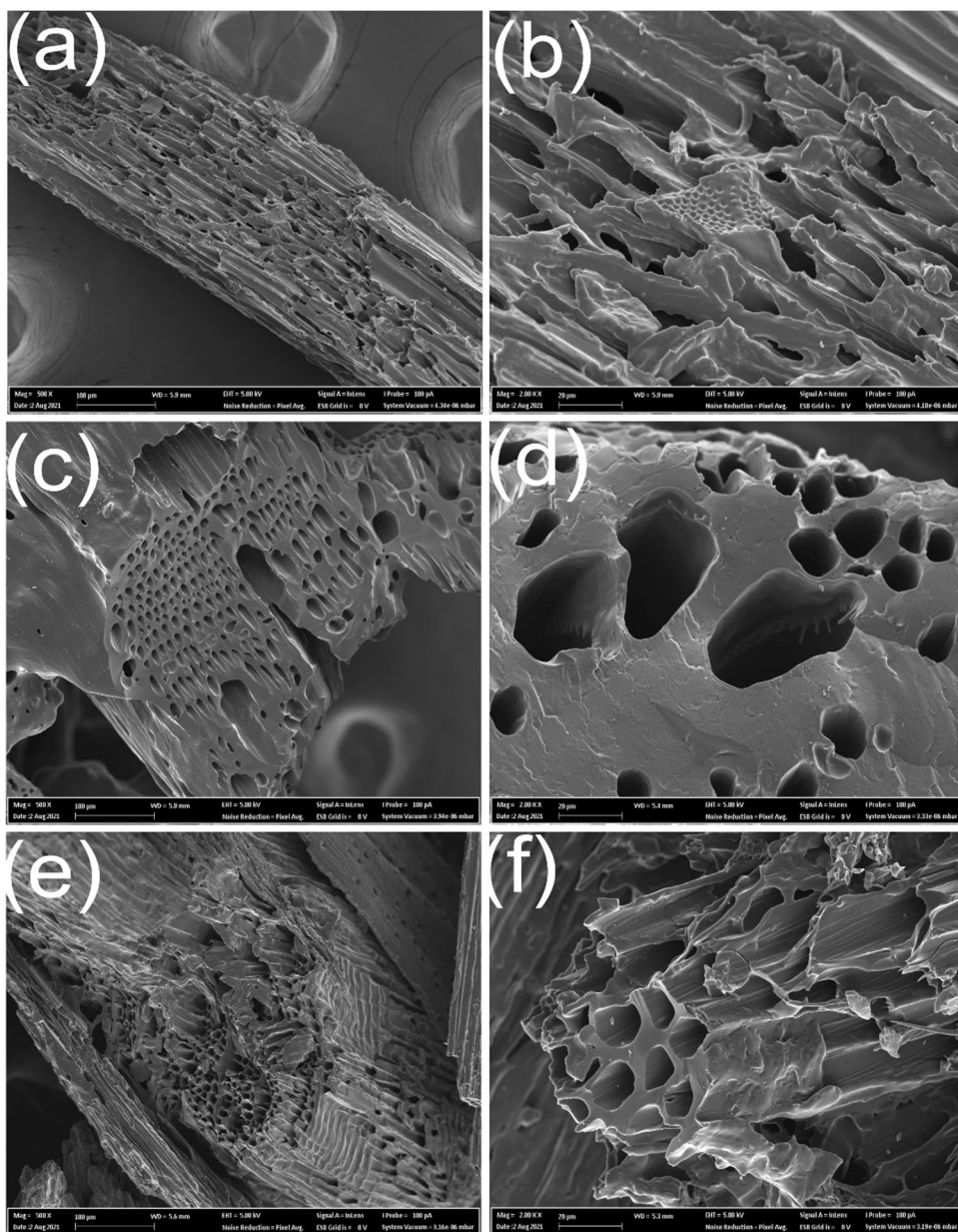
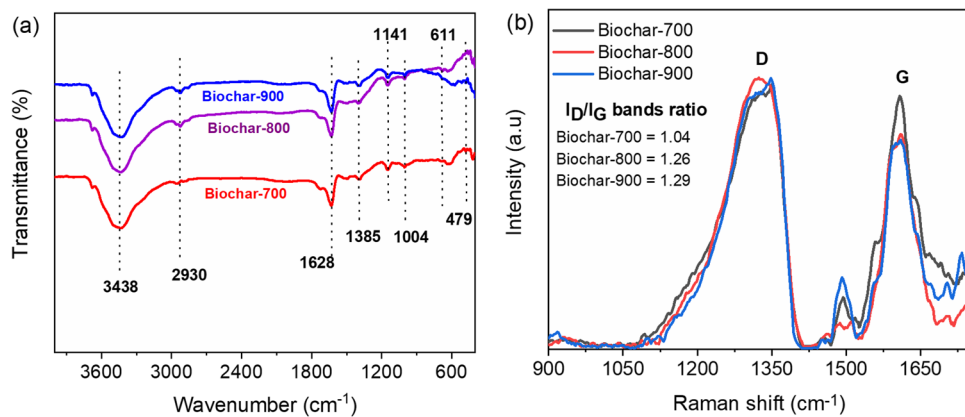


Fig. 3 FTIR (a) and Raman (b) spectra of the biochars



The functional groups present in the biochars are shown in Fig. 3a.

The spectra identified the presence of –OH stretching vibration at 3438 cm^{-1} . At 2930 cm^{-1} , it can be assigned to the C–H group stretching vibrate in long-chain aliphatic components [40, 41], while the peak at 1628 cm^{-1} is related to C=O from carboxylic compounds [41]. At 1141 and 1004 cm^{-1} , the amino phosphonic acid functional group and P–OH bonds can be assigned, demonstrating that a reaction occurred between H_3PO_4 and the precursor matrix to form biochar-700, biochar-800, and biochar-900 [40]. The addition of P-containing functional groups on biochars surfaces might positively affect the acetaminophen adsorption. In addition, the peaks at 611 and 479 cm^{-1} could be assigned to the C–H of alkenes and alkanes.

Raman spectroscopy analysis was performed to evaluate the degree of graphitization of the prepared biochars. From the spectra was determined the I_D/I_G band ratio

(Fig. 3b) calculated using the area under each peak. The lower I_D/I_G value indicates that biochar exhibits a more perfect and orderly graphite structures with a high graphitization degree [42], while a higher I_D/I_G reveals more structural defects in carbon materials. Moreover, I_D/I_G values also serve to identify the size of the sp^2 domain related to graphite structure in the biochar structure [39, 42]. Figure 3 b shows that the pyrolysis temperature did influence the graphitization degree of the biochars. The I_D/I_G band ratios were 1.04 (700 °C), 1.26 (800 °C), and 1.29 (900 °C), respectively. These values suggest a lower degree of graphitization of biochars resulting from the abundant presence of structural defects such as bonding disorders, vacancies, and heteroatoms in the graphene layers [42] as the pyrolysis temperature is increased. These defects may help provide more adsorption sites, which reflect better adsorption properties.

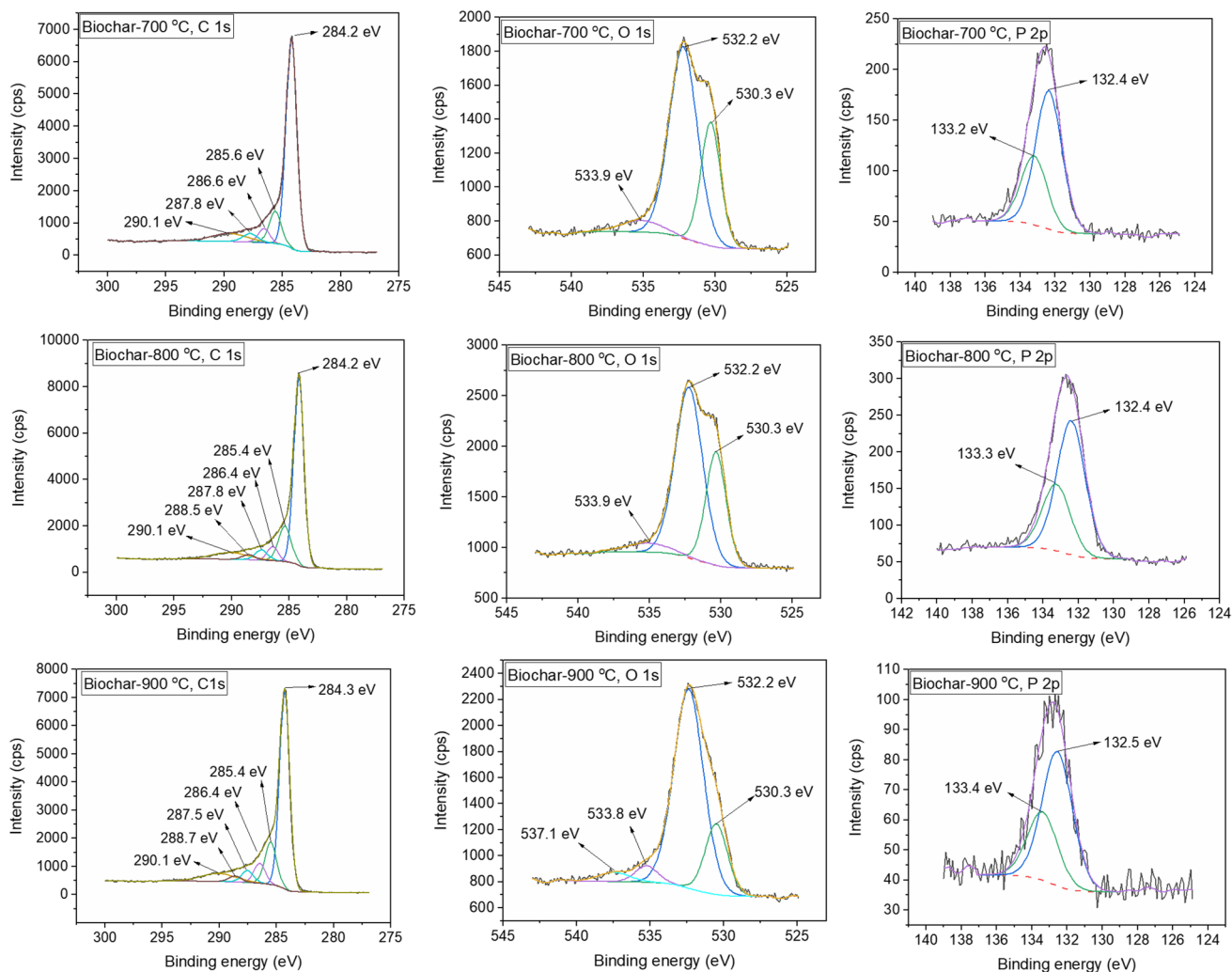


Fig. 4 XPS spectra of the C 1 s, O 1 s, and P 2p for the produced biochars

The elemental composition and chemical state of the biochars were evaluated through XPS analysis. XPS spectra provide more details on different surface modifications caused by oxidative-acidic treatments. Figure 4 shows C 1 s, O 1 s, and P 2p_{3/2} spectra, carbon, oxygen, and phosphorus bonds, respectively.

For all the investigated biochar samples, at least six forms of carbon occurring on the surface can be found (Fig. 4). The deconvolution of the C 1 s spectra shows bands at 284.2 eV which is assigned to graphitic carbon. The bands at 285.4–286.6 eV can be attributed to phenols ethers or alcohols (C–O–) and C–P bonds. At 287.5–287.8 eV, the bands can be attributed to carbonyl, quinone, or carbon bonded to nitrogen structures (C=O, C–N). At 288.5–288.7 eV, the bands are usually assigned to carboxylic groups or esters (COO). Moreover, the band at 290.1 eV is assigned to carbonates, occluded CO, or π -electrons in aromatic rings (C=O/C=C) [43–45].

These structures are confirmed by O 1 s spectra (Fig. 4) which shows bands at 530.3 eV, which might correspond to oxygen singly bonded to carbon and phosphorus groups (C–O–P groups), or metal oxides [43–45]; C=O bonds can be assigned at around 532 eV [43–45], and the band at around 533.9 eV is usually assigned to oxygen singly bonded to carbon in phenols and ethers [45]. The band at around 537 eV seen in the biochar-900 °C is occluded CO or CO₂ [45].

For the P 2p spectra, a band at 132.4 or 132.5 eV is observed in all three biochars that is commonly assigned to phosphate species in which P atom is bonded to O atoms (P–OH and or C–O–PO₃) [43, 44, 46], which is in agreement with the FT-IR results. The presence of P chemical bonds was also evidenced in the O 1 s spectrum (Fig. 4). Another band at 133.2–133.4 eV is also observed in the three biochars, which is attributed to C–PO₃ and or C₃–PO [44, 46]. The presence of P is related to the H₃PO₄ activation process, which acted also as P-doping process and can result in better adsorption properties.

The quantitative information for the main elements, from XPS, is shown in Table 3. The amount of C presented on the three biochars was high and had no significant variance. The O content also showed no big variance and presented high values for all samples. About the P-functional groups, as the temperature increased, the presence of P decreased; a large number of functionalities on the biochars' surfaces

(especially for functional groups related to C=O, C–OH, and P=O (see Table 3) can result in better adsorption performances.

3.2 Adsorption results

3.2.1 Influence of the biochar mass on acetaminophen removal

The adsorbent mass or dosage effect on the adsorption process is crucial for making the adsorption process applicable on an industrial scale because it avoids waste generation and minimizes costs associated with the process [47, 48].

The biochar's mass effect on acetaminophen removal was carried out varying amounts of biochar from 20 to 80 mg in 20 mL of acetaminophen solution, at an initial concentration of 200 mg L⁻¹, 6 h of agitation, pH 6.0, and temperature of 23 °C. The results obtained are presented in Fig. 5.

The percentage of removal increases as the biochar mass increases and its maximum (100%) was obtained for masses of 50.0, 60.0, and 70.0 mg for biochar-900, biochar-800, and biochar-700, respectively. Figure 5 shows that the acetaminophen percentage of removal increases, from 52 to 100%, as the biochar-700 mass is increased from 20 to 70 mg, respectively. For the biochar-800, the percentage of removal increased from 56.0 to 100.0% when the mass was increased from 20.0 to 60.0 mg, while for biochar-900, the percentage of removal increased from 68.0 to 100.0% when the mass increased from 20.0 to 50.0 mg. The highest efficiencies followed the highest SSA values, biochar-700, biochar-800, and biochar-900, respectively (see Fig. 5).

Increased biochar mass led to an increase in the available area and adsorption sites responsible for the adsorption process, and, therefore, the adsorption increased [47, 48]. On the other hand, for the adsorption capacity, an increase in the biochar's mass led to a continuous decrease in the *q* value as the adsorbent mass increases. This phenomenon could be mathematically explained by Eq. 12.

$$q = \frac{\% \text{Removal} \cdot C_0 \cdot V}{100 \cdot m} \quad (12)$$

Considering that when the percentage of removal attains a plateau (its value becomes practically constant) and that the value of volume and initial concentration of the

Table 3 Elemental composition of the biochars based on XPS analysis

Samples	C 1 s	O 1 s	N 1 s	P 2p _{3/2}	O 1 s species		
					C–O	C=O	P=O
Biochar-700	85.38	11.28	0.89	2.02	7.31	0.66	3.31
Biochar-800	83.65	12.99	0.84	2.2	8.25	0.72	4.02
Biochar-900	85.98	12.29	0.88	0.66	8.88	1.03	2.38

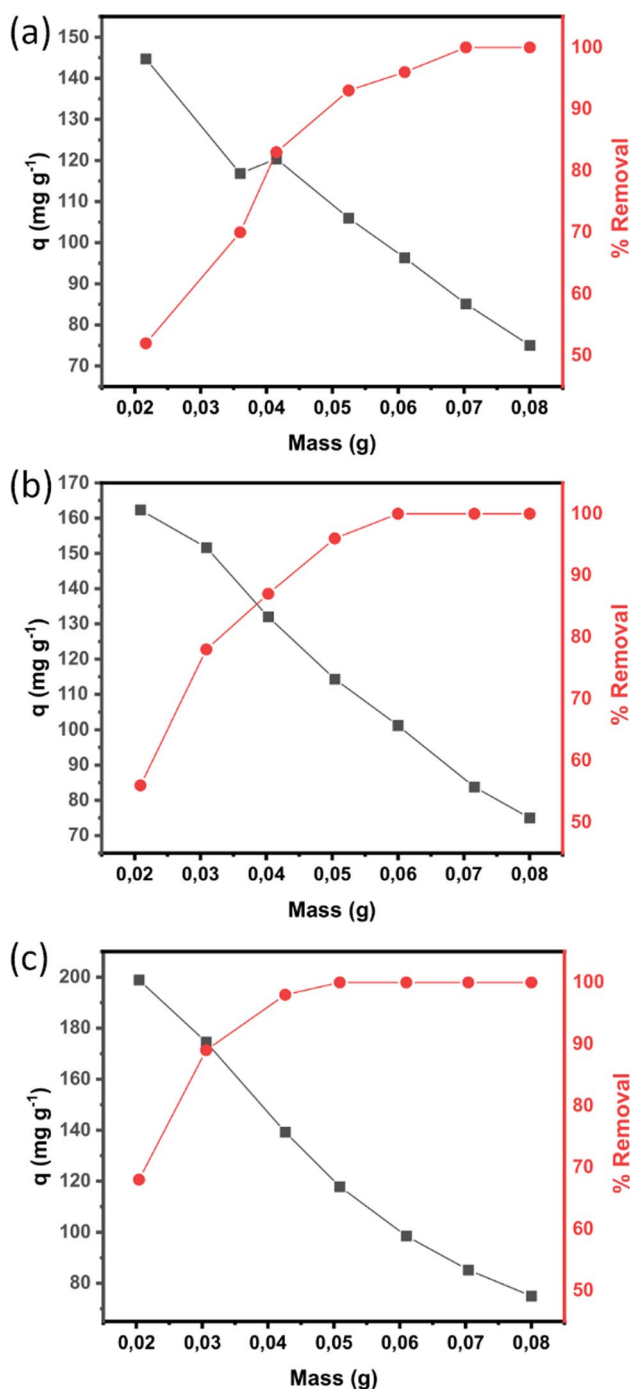


Fig. 5 Influence of the biochar mass on acetaminophen removal **a** biochar-700, **b** biochar-800, and **c** biochar-900. Adsorption experimental conditions: the initial adsorbate concentration was 200 mg L⁻¹, contact time of 6 h; temperature of 22 °C; initial pH adsorbate solution was 6.0 (natural solution pH)

pharmaceutical are fixed values, the sorption capacity is inversely proportional to the mass of the adsorbent.

Based on biochar mass studies, the optimal mass amount of the biochars was set up to be 40.0 mg (2.0 g L⁻¹). At this dosage, the removal capacities were 83, 87, and 98%

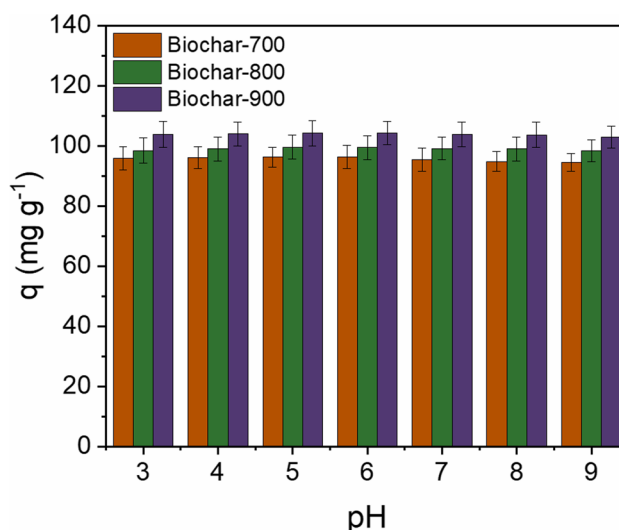


Fig. 6 Influence of initial pH on the acetaminophen removal. Adsorption experimental conditions: the initial adsorbate concentration was 200 mg L⁻¹, contact time of 6 h, temperature of 22 °C, adsorbent dosage of 2.0 g L⁻¹

for biochar-700, biochar-800, and biochar-900, respectively, practically attaining a plateau. This choice is justified because using a mass amount higher than 40 mg would not considerably improve the removal capacity [46, 47].

Therefore, for further adsorption experimental studies (effect of the pH, kinetic and isotherm studies and effluent treatment), the mass of biochar was fixed at 40.0 mg in 20.0 mL of adsorbate solution (2.0 g L⁻¹).

3.2.2 Influence of pH of acetaminophen solution on its adsorption process

The role of pH in acetaminophen ionization is significant due to the presence of different functional groups on the biochars' surfaces [25]. Figure 6 shows the adsorption capacity vs. the pH of the acetaminophen solution. It can be seen that for pH values 3–9, the q values were practically constant. These outcomes suggest that the adsorption mechanism for acetaminophen on the prepared biochars should not be electrostatic since it is not pH-dependent [25, 27]. Instead, pore-filling should be the most dominant mechanism of adsorption, which will be discussed later.

These results are supported by literature. Saucier et al. [25] prepared magnetic biochar and applied them for adsorption of acetaminophen. They varied the pH from 3 to 10 and found that the removal was practically constant within this pH interval. No pH influence was detected.

Based on the pH studies, further adsorption experiments were carried out with acetaminophen solutions with pH 6.0 (pH of the used deionized water); therefore, it was unnecessary to make any pH adjustments if the solution remains

within pH 3.0–9.0. The same is true for the synthetic effluents.

3.2.3 Kinetic studies

Kinetics of adsorption is an essential factor in determining the adsorption mechanism, associated with other data of characterization of the adsorbent and adsorbate and the equilibrium studies. The adsorption kinetics of acetaminophen on the biochars was explored using nonlinear pseudo-first-order, pseudo-second-order, and Avrami fractional-order kinetic models.

The kinetic curves and fitting parameters of the models are shown in Fig. 7 and Table 4, respectively. The suitability of the models was evaluated through the adjusted determination coefficient (R^2_{Adj}) and standard deviation (SD) [27,

38, 39, 47–49]. Lower SD and higher R^2_{Adj} values show a reduced disparity between experimental and theoretical q values and, therefore, higher suitability of the model [38, 39, 49–51]. Based on that, the Avrami fractional-order model was the most suitable because it presented the highest R^2_{adj} and lowest SD values for the three biochars (Table 4).

These results indicate that the Avrami fractional-order explained better the adsorption process of acetaminophen by all three biochars. The Avrami model indicates that the adsorption is complex, and the adsorption mechanisms follow different pathways [50, 51]. To further understand the adsorption process, intraparticle diffusion graphs are also shown (see Fig. 7 d, e, and f). The adsorption dynamics included three stages. The first stage can be related to boundary diffusion, where the adsorbate diffused on the adsorbent exterior surface [36, 52]. Intraparticle diffusion

Fig. 7 Kinetic (a, b, and c) and intraparticle (d, e, and f) curves for acetaminophen adsorption on the biochars. a, d Biochar-700, b, e biochar-800, and c, f biochar-900. Adsorption experimental conditions: the initial adsorbate concentration was 200 mg L⁻¹, temperature of 22 °C, adsorbent dosage of 2.0 g L⁻¹, initial pH adsorbate solution 6.0

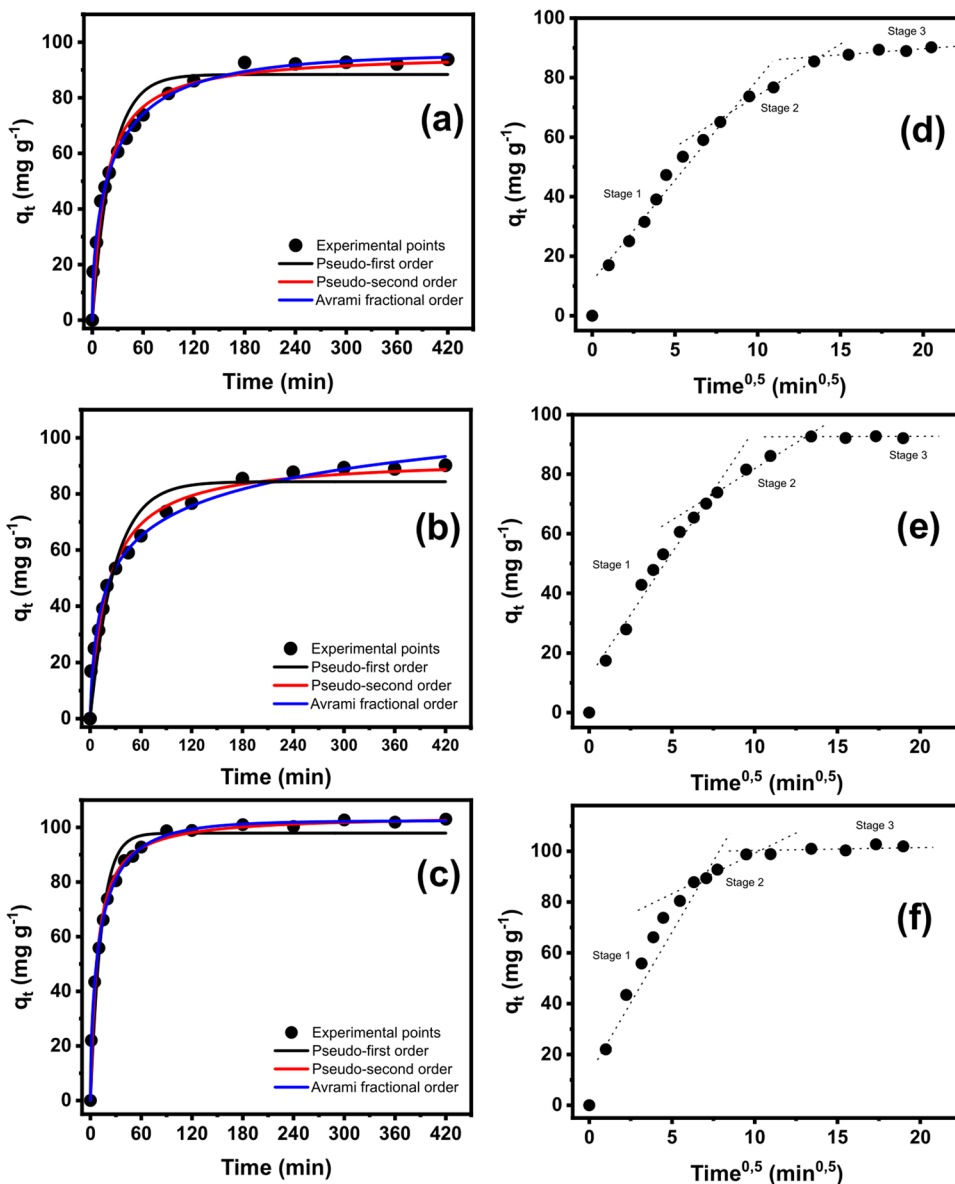


Table 4 Kinetic parameters of acetaminophen onto the biochar samples

Model	Acetaminophen initial concentration (200 mg L ⁻¹)		
	Biochar-700	Biochar-800	Biochar-900
Pseudo-first-order			
q_1 (mg g ⁻¹)	84.36	88.38	97.89
k_1 (min ⁻¹)	0.3514	0.4401	0.7844
R^2_{adj}	0.9366	0.9369	0.9567
SD (mg g ⁻¹)	7.294	7.284	6.413
Pseudo-second-order			
q_2 (mg g ⁻¹)	93.03	96.14	104.5
k_2 (g mg ⁻¹ min ⁻¹)	0.0005304	0.0006938	0.001220
R^2_{adj}	0.9760	0.9805	0.9899
SD (mg g ⁻¹)	4.487	4.053	3.099
Avrami fractional-order			
q_n (mg g ⁻¹)	94.22	95.89	102.5
k_{AV} (min ⁻¹)	0.002641	0.002150	0.07247
n_{AV} (-)	0.6321	0.5454	0.5778
R^2_{adj}	0.9943	0.9965	0.9987
$t_{0.5}$ (min)	18.92	14.10	7.39
$t_{0.95}$ (min)	183.2	158.3	82.2
SD (mg g ⁻¹)	2.022	1.701	1.129

into the pores of the adsorbent represents the second stage [36, 52]. In the third stage, the acetaminophen was adsorbed and diffused into the interior site of the biochars (through smaller pores), which is followed by the attainment of equilibrium [36, 52].

Further evaluating the kinetic process, $t_{0.5}$ and $t_{0.95}$ were studied. The values were calculated from the best model, Avrami. They represent the time (min) when 50% and 95% of saturation (q_e) is attained, respectively [47, 48]. For biochar-700, $t_{0.5}$ was 18.92, and $t_{0.95}$ was 183.2 min. For biochar-800 and biochar-900, the values were 14.10 ($t_{0.5}$) and 158.3 ($t_{0.95}$) and 7.39 ($t_{0.5}$) and 82.2 ($t_{0.95}$), respectively (see Table 4).

Due to the biochar-900 textural properties and chemical surface features, it had a faster kinetic of adsorption when the values of $t_{0.5}$ and $t_{0.95}$ are considered. Biochar-900 displayed the highest SSA and higher amount of micro and mesopores (see Table 2), and this can explain the better efficiency in the adsorption process.

The adsorption work was further continued by establishing the contact times such as 3.5 h. The established contact time was slightly higher than the $t_{0.95}$ to ensure that the adsorption process had enough time to reach the equilibrium between acetaminophen and biochars because $t_{0.95}$ will attain 95% saturation; the equilibrium should be established when the complete saturation of the adsorbent is attained.

3.2.4 Equilibrium studies

Equilibrium of adsorption is one of the most critical pieces of information for the correct understanding of an adsorption process. Therefore, it is crucial to understand the adsorption mechanism pathways and effective design of the adsorption system [27, 38, 39, 47–49]. Therefore, the equilibrium system between acetaminophen and the biochars was evaluated using the nonlinear fitting of Langmuir, Freundlich, and Liu models and the obtained data are displayed in Fig. 8 and Table 5, respectively.

The suitability of the equilibrium models was evaluated in the same way as for the kinetic studies (through R^2_{Adj} and SD values). Based on that, the Liu isotherm model was the most suitable model for all three biochars because it presented the highest R^2_{Adj} and lowest SD values. It was, therefore, used to describe the relationship between acetaminophen and the biochars adsorption system.

This isotherm model can be applied to both homogenous and heterogeneous systems, and it has a hybrid adsorption mechanism, which does not follow ideal monolayer adsorption. This is highlighted because Freundlich did not provide a good fit for the experimental adsorption data (see Fig. 8 and Table 5). This suggests that the adsorption process of acetaminophen on the three biochars was more homogenous than heterogeneous.

3.2.5 Acetaminophen mechanism of adsorption

Based on the porosity, chemical characterization and adsorption data such as SSA, pore size distribution, surface functionalities, initial pH solution, the kinetics of adsorption, and equilibrium studies, the possible acting mechanisms of adsorption of acetaminophen on the biochars are suggested in Fig. 9.

It can be stated that electrostatic attraction was not the primary mechanism acting between acetaminophen and the biochars since it depends on pH, and it was shown that the pH did not influence the acetaminophen removal. However, some interactions such as van der Waals (hydrophobic interactions, π - π stacking), hydrogen bonds, and polar interactions of the oxygen and nitrogen groups of the acetaminophen with the polar groups of the biochars took place [35, 49]. In addition, Nguyen et al. [53] also reported a minor contribution of weak van der Waals force in the adsorption mechanism of acetaminophen on biochars.

The major mechanism that took place on the acetaminophen removal was the pore-filling due to the well-developed pore structure and elevated SSA values. Therefore, the pore-filling largely contributed to the high efficiency of acetaminophen adsorption (Fig. 9).

Due to the dimensions of the acetaminophen molecule (1.19 nm (length), 0.75 nm (width), and 0.46 nm

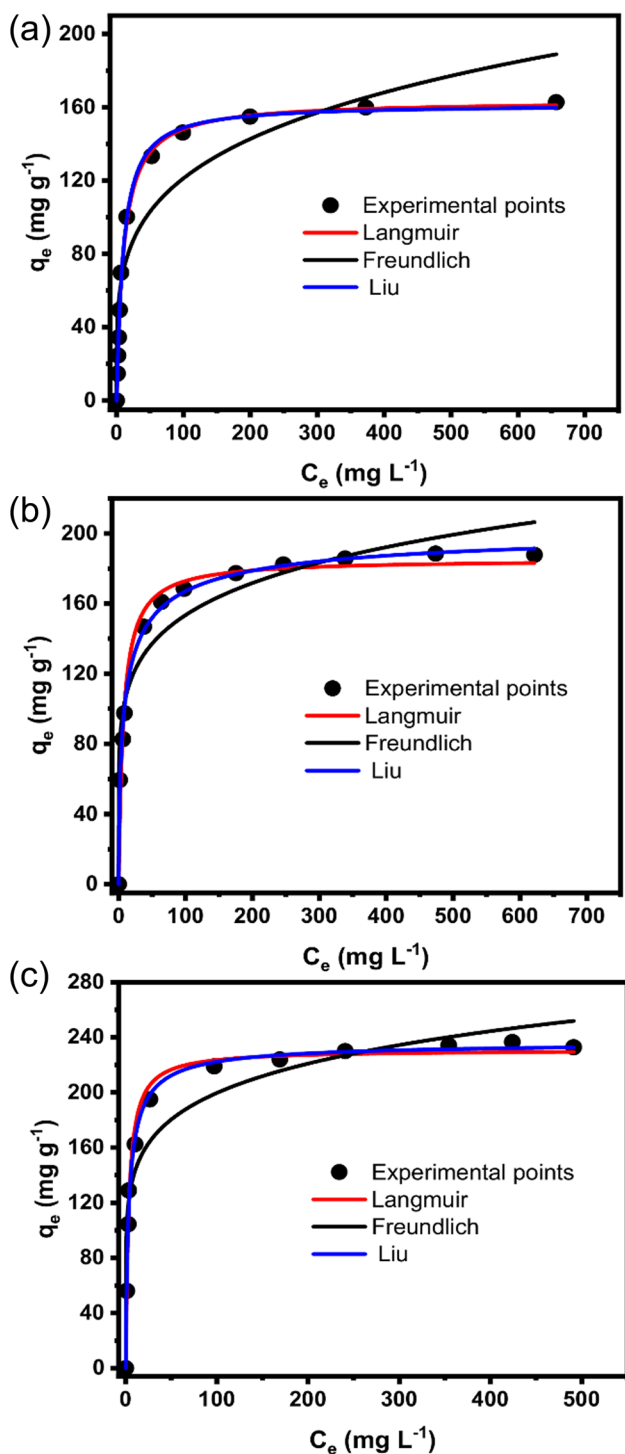


Fig. 8 Isotherm curves for acetaminophen adsorption on the biochar-700 (a), biochar-800 (b), and biochar-900 (c). Adsorption experimental conditions: the initial adsorbate concentration from 10 to 1000 mg L⁻¹, contact time of 3.5 h, temperature of 22 °C, adsorbent dosage of 2.0 g L⁻¹, initial pH adsorbate solution 6.0

(thickness)), it is expectable that it can easily access the wider and also some of the narrower micropores. Galhetas et al. [54] reported that the affinity of acetaminophen

Table 5 Equilibrium parameters of acetaminophen onto the biochar samples

Model	Samples		
	Biochar-700	Biochar-800	Biochar-900
Langmuir			
Q_{max} (mg g ⁻¹)	163.6	185.3	231.0
k_L (L mg ⁻¹)	0.09581	0.1399	0.3029
R^2_{adj}	0.9967	0.9766	0.9901
SD (mg g ⁻¹) ²	3.563	9.481	7.943
Freundlich			
k_F ((mg g ⁻¹)(mg L ⁻¹) ^{-1/nF})	40.98	72.62	102.0
n_F (dimensionless)	4.246	6.155	6.854
R^2_{adj}	0.8747	0.9482	0.9239
SD (mg g ⁻¹) ²	22.03	14.11	21.99
Liu			
Q_{max} (mg g ⁻¹)	161.4	205.7	236.8
K_g (L mg ⁻¹)	0.1012	0.1068	0.2817
n_L (dimensionless)	1.066	0.6186	0.8187
R^2_{adj}	0.9968	0.9954	0.9922
SD (mg g ⁻¹) ²	3.540	4.224	7.042

molecules is maximized by pores centered at pore widths near 0.7 nm. Table 2 shows that our biochars presented large portions of mesopores that facilitate the acetaminophen adsorption.

3.2.6 Synthetic wastewater treatment tests

Considering the excellent properties of the biochars for acetaminophen removal, it is expected that all three biochars could be effectively employed in the treatment of wastewaters composed of compounds commonly found in effluents from hospitals or pharmaceutical industries. Therefore, two synthetic wastewaters with seven drugs and other organic and inorganic compounds, usually found in wastewaters (Table 1), were employed to test the ability of the biochars to clean them up (Fig. 10).

The results showed, for the three biochars, interesting percentage of removals for both effluents. For effluent A, percentages were 68.6%, 74.2%, and 76.3% for biochar-700, biochar-800, and biochar-900, respectively, while for the effluent B, the percentages were 76.4%, 81.6%, and 84.7% for biochar-700, biochar-800, and biochar-900, respectively. Thus, the results strongly support the practical application of the biochars in treating real pharmaceutical wastewaters.

3.2.7 Regeneration studies

The biochar with the better acetaminophen removal performance (biochar-900) was used to evaluate the regeneration

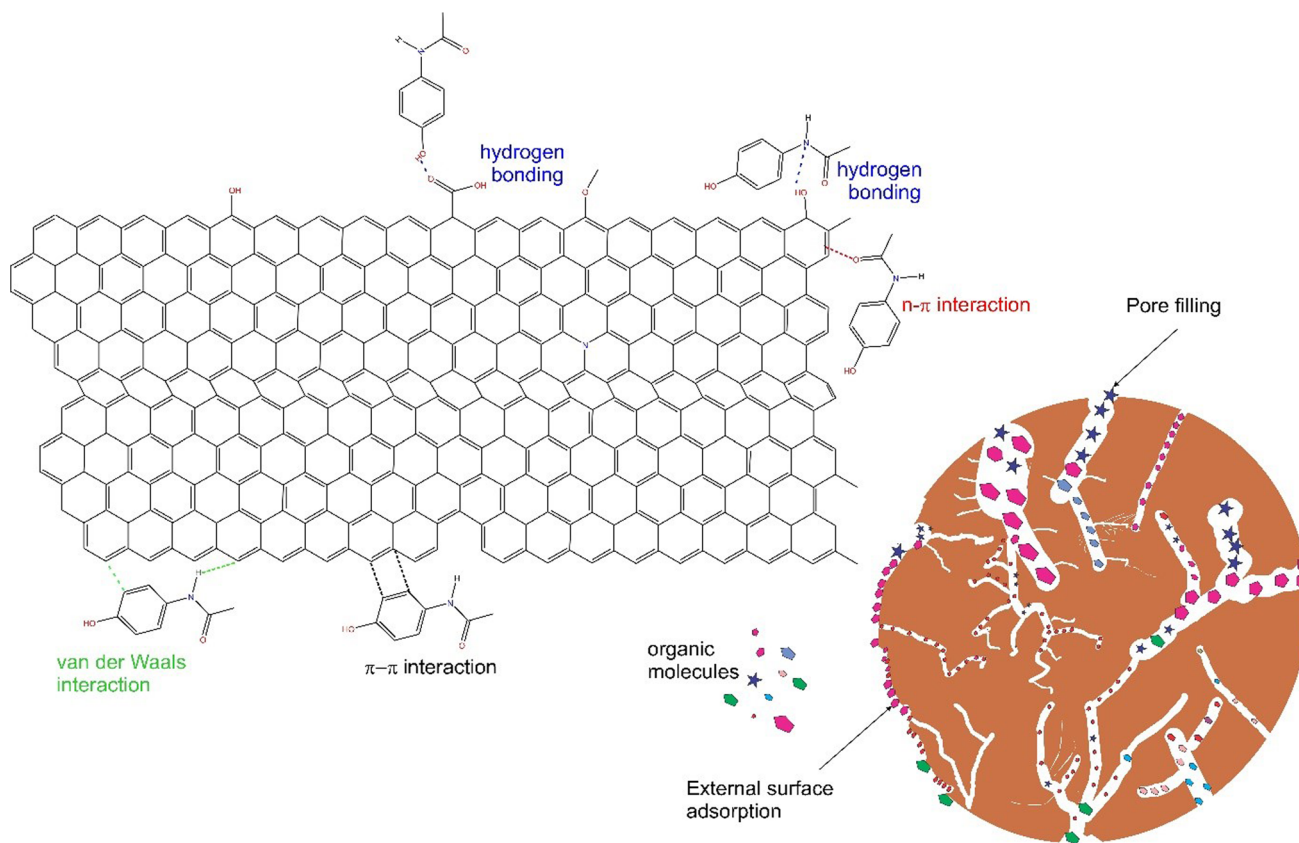


Fig. 9 Mechanism of adsorption for acetaminophen on the biochar matrix

studies. The sample was tested in four adsorption–desorption cycles. The tests were performed at an acetaminophen initial concentration of 300 mg L^{-1} , an adsorbent dosage of 2.0 g L^{-1} , and two eluents were employed (solutions of $0.1 \text{ M NaOH} + 20\% \text{ EtOH}$ and $0.25 \text{ M NaOH} + 20\% \text{ EtOH}$).

Figure 11 shows that the eluent $0.1 \text{ M NaOH} + 20\% \text{ EtOH}$ resulted in a better recyclability efficiency. The worse efficiency for the $0.25 \text{ M NaOH} + 20\% \text{ EtOH}$ eluent could be explained by the fact that the higher concentration of NaOH could compete with the acetaminophen molecules, cover the biochar surface, and get trapped into the small pores of the biochar [27] (17.7% of the SSA is composed of micropores, see Table 2).

With the eluent $0.1 \text{ M NaOH} + 20\% \text{ EtOH}$, the 2nd cycle adsorbed roughly 70% of the acetaminophen, while in the 4th cycle, the removal was approximately 44%. This decrease could be caused by acetaminophen molecules seized in the small pores of the biochar, which is difficult to be removed by the eluent [27].

To sum up, the biochars exhibited good reusability for a second cycle. However, further experiments on testing different eluents could help the biochar to reach even higher adsorption performances after two or more cycles.

4 Conclusions

In this work, birch wood–based spent mushroom substrate (SMS) was employed as a precursor to prepare highly porous biochars using a single step activation procedure with phosphoric acid (H_3PO_4) as a chemical activator. The main results from this research can be summarized as follows:

1. The pyrolysis temperature influenced, positively, the porosity of the biochars. The specific surface areas (SSA) were $975 \text{ m}^2 \text{ g}^{-1}$ ($700 \text{ }^\circ\text{C}$), $1031 \text{ m}^2 \text{ g}^{-1}$ ($800 \text{ }^\circ\text{C}$), and $1215 \text{ m}^2 \text{ g}^{-1}$ ($900 \text{ }^\circ\text{C}$).
2. The biochars presented a very high percentage of mesopores in their structures, 75.4% ($700 \text{ }^\circ\text{C}$), 78.5% ($800 \text{ }^\circ\text{C}$), and 82.3% ($900 \text{ }^\circ\text{C}$).
3. Chemical characterization of the biochars indicated disordered carbon structures with the presence of oxygen and phosphorous functional groups on their surfaces.
4. The kinetic data were fitted to the Avrami fractional-order model and equilibrium of adsorption data was well represented by the Liu isotherm model, attaining a very high adsorption capacity of 236.8 mg g^{-1} for the sample pyrolyzed at $900 \text{ }^\circ\text{C}$.

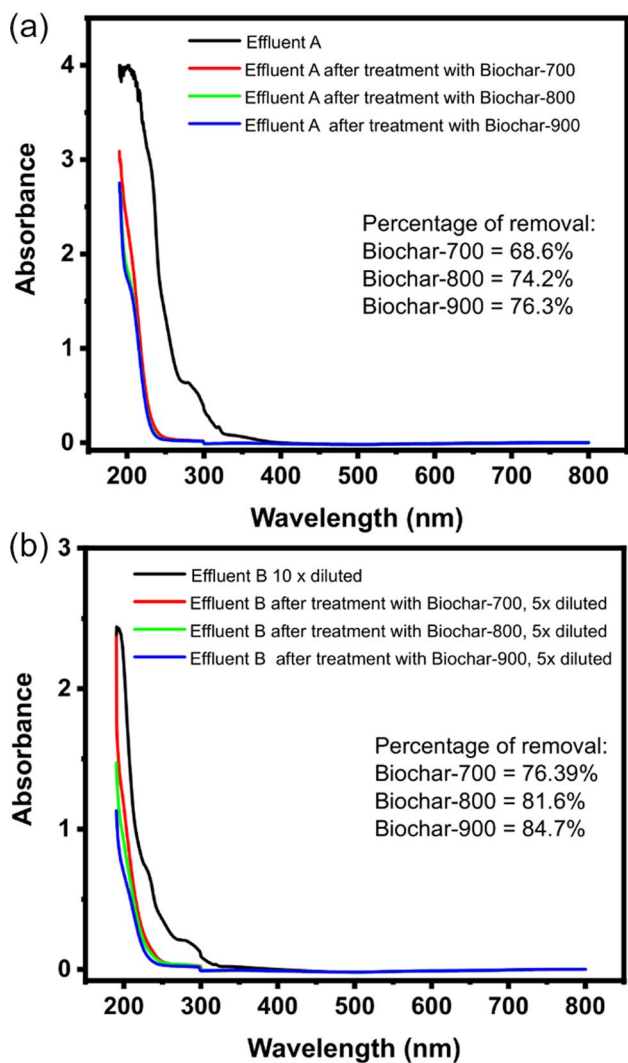


Fig. 10 Effluents spectra of non-treated and treated with biochar-700, biochar-800, and biochar-900. For the composition of effluents A and B, see Table 1

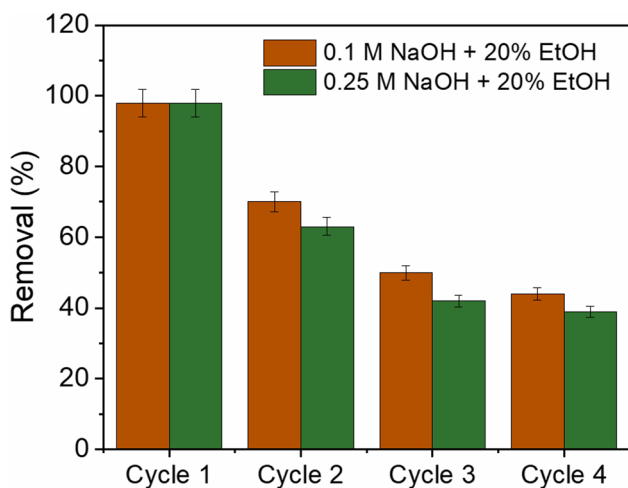


Fig. 11 Cycles of adsorption of acetaminophen onto biochar-900

- The adsorption mechanism suggests that the pore-filling mechanism mainly dominates the acetaminophen removal, although van der Waals forces are also involved in the process.
- The employment of the biochars in the treatment of simulated pharmaceutical effluents showed a high percentage of removal (up to 84.7%).
- The biochars can be regenerated using 0.1 M NaOH + 20% EtOH solution as an eluent; however, the percentage of removal was reduced by approximately 50% after three adsorption–desorption cycles.

The above results strongly suggest that birch wood-based SMS was a highly efficient precursor for biochar preparation, which could be effectively used to treat real effluents containing micropollutants.

Acknowledgements We thank Bio4Energy, a Strategic Research Environment appointed by the Swedish government, as well as the Swedish University of Agricultural Sciences for supporting this work. The Umeå Core Facility for Electron Microscopy (UCEM-NMI node) and the Vibrational Spectroscopy Core Facility (ViSp) at the Chemical Biological Centre (KBC), Umeå University, are gratefully acknowledged. The Wallenberg Wood Science Center (WWSC) is gratefully acknowledged. This work is also a part of the Johan Gadolin Process Chemistry Centre at Åbo Akademi University. The authors want to thank Alexandr Talyzin, Department of Physics, Umeå University, for the valuable comments on the manuscript.

Author contribution Alejandro Grimm: conceptualization, methodology, investigation, data curation, writing -original draft, funding acquisition. Glaydson S. dos Reis: data curation, writing — original draft. Van Minh Dinh: data curation, formal analysis. Sylvia H. Larsson: resources. Jyri-Pekka Mikkola: writing — review and editing. Eder C. Lima: writing — review and editing. Shaojun Xiong: writing — review and editing, funding acquisition.

Funding Open access funding provided by Swedish University of Agricultural Sciences. This research was funded by the Re:source program (P42481) and BioInnovation (2017–02705), co-financed by the Swedish State Innovation Department (VINNOVA), the Swedish Energy Agency, and the Swedish Research Council FORMAS (2021–00877).

Declarations

Conflict of interest The authors declare no competing interests.

Open Access This article is licensed under a Creative Commons Attribution 4.0 International License, which permits use, sharing, adaptation, distribution and reproduction in any medium or format, as long as you give appropriate credit to the original author(s) and the source, provide a link to the Creative Commons licence, and indicate if changes were made. The images or other third party material in this article are included in the article's Creative Commons licence, unless indicated otherwise in a credit line to the material. If material is not included in the article's Creative Commons licence and your intended use is not permitted by statutory regulation or exceeds the permitted use, you will need to obtain permission directly from the copyright holder. To view a copy of this licence, visit <http://creativecommons.org/licenses/by/4.0/>.

References

- Jones OAH, Voulvoulis N, Lester JN (2004) Potential ecological and human health risks associated with the presence of pharmaceutically active compounds in the aquatic environment. *Crit Rev Toxicol* 34:335–350
- Sophia CA, Lima EC (2018) Removal of emerging contaminants from the environment by adsorption. *Ecotoxicol Environ Saf* 150:1–17
- NORMAN (2022) The network of reference laboratories, research centres and related organisations for monitoring of emerging environmental substances, www.norman-network.net. Accessed March 2022.
- Borrull J, Colom A, Fabregas J, Borrull F, Pocurrull E (2021) Presence, behaviour and removal of selected organic micro-pollutants through drinking water treatment. *Chemosphere* 276:130023
- Deere JR, Moore S, Ferrey M, Jankowski MD, Convertino M, Servadio JL, Phelps NBD, Hamilton MC, Chenux-Ibrahim Y, Travis DA, Wolf TM (2020) Occurrence of contaminants of emerging concern in aquatic ecosystems utilized by Minnesota tribal communities. *Sci Total Environ* 724:138057
- Bunting SY, Lapworth DJ, Crane EJ, Grima-Olmedo J, Korosa A, Kuczynska A, Mali N, Rosenqvist L, van Vliet ME, Togola A, Lopez B (2021) Emerging organic compounds in European groundwater. *Environ Pollut* 269:115945
- Yu X, Sui Q, Lyu S, Zhao W, Liu J, Cai Z, Yu G, Barcelo D (2020) Municipal solid waste landfills: an underestimated source of pharmaceutical and personal care products in the water environment. *Environ Sci Technol* 54:9757–9768
- Kapelewska J, Kotowska U, Karpińska J, Kowalczyk D, Arciszewska A, Świrnydo A (2018) Occurrence, removal, mass loading and environmental risk assessment of emerging organic contaminants in leachates, groundwaters and wastewaters. *Microchem J* 137:292–301
- Santos LHMLM, Araújo AN, Fachini A, Pena A, Delerue-Matos C, Montenegro MCBSM (2010) Ecotoxicological aspects related to the presence of pharmaceuticals in the aquatic environment. *J Hazard Mater* 175:45–95
- Bio S, Nunes B (2020) Acute effects of diclofenac on zebrafish: indications of oxidative effects and damages at environmentally realistic levels of exposure. *Environ Toxicol Phar* 78:103394
- Gros M, Petrović M, Ginebreda A, Barceló D (2010) Removal of pharmaceuticals during wastewater treatment and environmental risk assessment using hazard indexes. *Environ Int* 36:15–26
- Ternes TA, Stüber J, Herrmann N, McDowel D, Ried A, Kampmann M, Teiser B (2003) Ozonation: a tool for removal of pharmaceuticals, contrast media and musk fragrances from wastewater? *Water Res* 37:1976–1982
- Mohanty K, Purkait MK (2012) Membrane technologies and applications. CRC Press, Taylor & Francis Group, LLC, Boca Raton, FL 33487–2742
- Della-Flora A, Wilde ML, Thue PS, Lima DR, Lima EC, Sirtori C (2020) Combination of solar photo-Fenton and adsorption process for removal of the anticancer drug Flutamide and its transformation products from hospital wastewater. *J Hazard Mater* 396:122699
- Della-Flora A, Mi W, Pinto IDF, Lima EC, Sirtori C (2020) Degradation of the anticancer drug flutamide by solar photo-Fenton treatment at near-neutral pH: identification of transformation products and in silico (Q)SAR risk assessment. *Environ Res* 183:109223
- Murrieta MF, Brillas E, Nava JL, Sirés I (2020) Photo-assisted electrochemical production of HClO and Fe²⁺ as Fenton-like reagents in chloride media for sulfamethoxazole degradation. *Sep Purif Technol* 250:117236
- Freitas JRLE, Quintão FJO, da Silva JCC, Silva SQ, Aquino SF, Afonso RJCF (2017) Characterisation of captopril photolysis and photocatalysis by-products in water by direct infusion, electrospray ionisation, high-resolution mass spectrometry and the assessment of their toxicities. *Int J Environ Anal Chem* 97:42–55
- Mahmoud WMM, Kümmerer K (2012) Captopril, and its dimer captopril disulfide: photodegradation, aerobic biodegradation, and identification of transformation products by HPLC–UV and LC–ion trap–MSn. *Chemosphere* 88:1170–1177
- Kovacic M, Papac J, Kusic H, Karamanis P, Loncaric BA (2020) Degradation of polar and non-polar pharmaceutical pollutants in water by solar assisted photocatalysis using hydrothermal TiO₂-SnS₂. *Chem Eng J* 382:122826
- dos Santos AJ, Cabot PL, Brillas E, Sires I (2020) A comprehensive study on the advanced electrochemical oxidation of antihypertensive captopril in different cells and aqueous matrices. *Appl Catal B* 277:119240
- Silva A, Delerue-Matos C, Figueiredo SA, Freitas OM (2019) The use of algae and fungi for removal of pharmaceuticals by bioremediation and biosorption processes: a review. *Water* 11:1555
- Wamba AGN, Ndi SK, Lima EC, Kayem JG, Thue PS, Costa TMH, Quevedo AB, Benvenuti EV, Machado FM (2019) Preparation, characterisation of titanate nanosheet–pozzolan nanocomposite and its use as an adsorbent for removal of diclofenac from simulated hospital effluent. *J Taiwan Inst Chem Eng* 102:321–329
- Dordio AV, Miranda S, Prates Ramalho JP, Palace Carvalho AJ (2017) Mechanisms of removal of three widespread pharmaceuticals by two clay materials. *J Hazard Mater* 323:575–583
- Sun K, Shi Y, Chen H, Wang X, Li Z (2017) Extending surfactant-modified 2:1 clay minerals for the uptake and removal of diclofenac from water. *J Hazard Mater* 323:567–574
- Saucier C, Karthickeyan P, Ranjithkumar V, Lima EC, dos Reis GS, de Brum IAS (2017) Efficient removal of amoxicillin and paracetamol from aqueous solutions using magnetic-activated carbon. *Environ Sci Pollut Res Int* 24:5918–5932
- dos Reis GS, Sampaio CH, Lima EC, Wilhelm M (2016) Preparation of novel adsorbents based on combinations of polysiloxanes and sewage sludge to remove pharmaceuticals from aqueous solutions. *Colloids Surf A* 497:304–315
- Lima DR, Hosseini-Bandegharai A, Thue PS, Lima EC, de Albuquerque YRT, dos Reis GS, Umpierrez CS, Dias SLP, Tran HN (2019) Efficient acetaminophen removal from water and hospital effluents treatment by activated carbons derived from Brazil nutshells. *Colloid Surf A* 583:123966
- Tran HN, Tomul F, Thi Hoang Ha N, Nguyen DT, Lima EC, Le GT, Chang CT, Masindi V, Woo SH (2020) Innovative spherical biochar for pharmaceutical removal from water: insight into adsorption mechanism. *J Hazard Mater* 394:122255
- Royse D, Baars JJP, Tan Q (2017) Current overview of mushroom production in the world. In: Zied D, Pardo-Giménez A (eds) *Edible and medicinal mushrooms: technology and applications*. Wiley, Singapore, pp 5–13
- Finney KN, Ryu C, Sharifi VN, Swithenbank J (2009) The reuse of spent mushroom compost and coal tailings for energy recovery: comparison of thermal treatment technologies. *Bioresour Technol* 100:310–315
- Zhang RH, Li XJ, Fadel JG (2002) Oyster mushroom cultivation with rice and wheat straw. *Bioresour Technol* 82:277–284
- Grimm A, Eilertsen L, Chen F, Huang R, Atterhem L, Xiong S (2021) Cultivation of *Pleurotus ostreatus* mushroom on substrates made of cellulose fibre rejects: product quality and spent substrate fuel properties. *Waste Biomass Valor* 12:4331–4340
- Caicedo DF, dos Reis GS, Lima EC, de Brum IAS, Thue PS, Cazacliu BG, Lima DR, dos Santos AH, Dotto GL (2020)

- Efficient adsorbent based on construction and demolition wastes functionalized with 3-aminopropyltriethoxysilane (APTES) for the removal ciprofloxacin from hospital synthetic effluents. *J Environ Chem Eng* 8:103875
34. Fröhlich AC, dos Reis GS, Pavan FA, Lima EC, Foletto EL (2018) Improvement of activated carbon characteristics by sonication and its application for pharmaceutical contaminant adsorption. *Environ Sci Pollut Res* 25:24713–24725
 35. Lima EC, Adebayo MA, Machado FM (2015) Chapter 3: kinetic and equilibrium models of adsorption, in carbon nanomaterials as adsorbents for environmental and biological applications. C.P. Bergmann, F.M. Machado, editors Springer International Publishing, 3369
 36. dos Reis GS, Adebayo M, Pascal ST, Sampaio CH, Lima EC, Dias SLP, De Brum IAS, Pavan F (2017) Removal of phenolic compounds from aqueous solutions using sludge-based activated carbons prepared by conventional heating and microwave-assisted pyrolysis. *Water Air Soil Pollut* 228:1–17
 37. Thommes M, Kaneko K, Neimark AV, Olivier JP, Rodriguez-Reinoso F, Rouquerol J, Sing KSW (2015) Physisorption of gases, with special reference to the evaluation of surface area and pore size distribution (IUPBBC technical report). *Pure Appl Chem* 87:1051–1069
 38. Cunha MR, Lima EC, Lima DR, da Silva RS, Thue PS, Seliem MK, Sher F, dos Reis GS, Larsson SH (2020) Removal of captopril pharmaceutical from synthetic pharmaceutical-industry wastewaters: Use of activated carbon derived from *Butia catarinensis*. *J Environ Chem Eng* 8:104506
 39. dos Reis GS, Larsson SH, Thyrel M, Pham TN, Lima EC, de Oliveira HP, Dotto GL (2021) Preparation and application of efficient biobased carbon adsorbents prepared from spruce bark residues for efficient removal of reactive dyes and colors from synthetic effluents. *Coatings* 11:772
 40. Liu L, Li Y, Fan S (2019) Preparation of KOH and H₃PO₄ modified biochar and its application in methylene blue removal from aqueous solution. *Processes* 7:891
 41. Lu Z, Zhang H, Shahab A, Zhang K, Zeng H, Bacha AUR, Nabi I, Ullah H (2021) Comparative study on characterization and adsorption properties of phosphoric acid activated biochar and nitrogen-containing modified biochar employing *Eucalyptus* as a precursor. *J Clean Prod* 303:127046
 42. Chen J, Mao Z, Zhang L, Tang Y, Wang D, Bie L, Fahlman BD (2018) Direct production of nitrogen-doped porous carbon from urea via magnesiothermic reduction. *Carbon* 130:41–47
 43. Li Y, Li S, Wang Y, Wang J, Liu H, Liu X, Wang L, Liu X, Xue W, Ma N (2017) Electrochemical synthesis of phosphorus-doped graphene quantum dots for free radical scavenging. *Phys Chem Chem Phys* 19:11631
 44. Li Y, Zhang X, Yang R, Li G, Hu C (2015) The role of H₃PO₄ in the preparation of activated carbon from NaOH-treated rice husk residue. *RSC Adv* 5:32626–32636
 45. Terzyk AP (2001) The influence of activated carbon surface chemical composition on the adsorption of acetaminophen (paracetamol) in vitro, part II. TG, FTIR, and XPS analysis of carbons and the temperature dependence of adsorption kinetics at the neutral pH. *Colloid Surface A* 177:23–45
 46. Cordero-Lanzac T, Palos R, Arandes JM, Castaño P, Rodríguez-Mirasol J, Cordero T, Bilbao J (2017) Stability of an acid activated carbon based bifunctional catalyst for the raw bio-oil hydrodeoxygenation. *Appl Catal B-Environ* 203:389–399
 47. dos Reis GS, Thue PS, Cazacliu BG, Lima EC, Sampaio CH, Quattrone M, Ovsyannikova E, Kruse A, Dotto GL (2020) Effect of concrete carbonation on phosphate removal through adsorption process and its potential application as fertilizer. *J. Clean. Prod.* 256:120416
 48. dos Reis GS, Cazacliu BG, Correa CR, Ovsyannikova E, Kruse A, Sampaio CH, Lima EC, Dotto GL (2020) Adsorption and recovery of phosphate from aqueous solution by the construction and demolition wastes sludge and its potential use as phosphate-based fertilizer. *J Environ Chem Eng* 8:103605
 49. Ferreira RC, Couto Junior OM, Carvalho KQ, Arroyo PA, Barros MASD (2015) Effect of solution pH on the removal of paracetamol by activated carbon of dende coconut mesocarp. *Chem Biochem Eng Q* 29:47–53
 50. Cestari AR, Vieira EFS, Vieira GS, Almeida LE (2006) The removal of anionic dyes from aqueous solutions in the presence of anionic surfactant using aminopropyl silica-a kinetic study. *J Hazard Mater* 138:133–141
 51. Lopes ECN, Dos Anjos FSC, Vieira EFS, Cestari AR (2003) An alternative Avrami equation to evaluate kinetic parameters of the interaction of Hg(II) with thin chitosan membranes. *J Colloid Interface Sci* 263:542–547
 52. Huang Y, Lee X, Grattieri M, Macazo FC, Cai R, Minter SD (2018) A sustainable adsorbent for phosphate removal: modifying multi-walled carbon nanotubes with chitosan. *J Mater Sci* 53:12641–12649
 53. Nguyen DT, Tran HN, Juang RS, Dat ND, Tomul F, Ivanets A, Woo SH, Hosseini-Bandegharai A, Nguyen VP, Chao HP (2020) Adsorption process and mechanism of acetaminophen onto commercial activated carbon. *J Environ Chem Eng* 8:104408
 54. Galhetas M, Mestre AS, Pinto ML, Gulyurtlu I, Lopes H, Carvalho AP (2014) Carbon-based materials prepared from pine gasification residues for acetaminophen adsorption. *Chem Eng J* 240:344–351

Publisher's note Springer Nature remains neutral with regard to jurisdictional claims in published maps and institutional affiliations.